CENTRAL ASIAN TRANSACTIONS ON MATERIALS STRUCTURE AND PROPERTIES

https://doi.org/10.51885/3134-7983_CATMSP_2026_2_8
SRSTI 53.39.00

INFLUENCE OF MECHANICAL ACTIVATION AND SPARK PLASMA SINTERING ON THE STRUCTURE AND PROPERTIES OF WC-FE AND WC-NI ALLOYS

Yerkezhan Tabiyeva [1], Dias Yerbolat [1]*, Azamat Urkunbay [1], Madina Aidarova [1], Sayat Zakerov [1], Małgorzata Rutkowska-Gorczyca [2]

[1]Center of Excellence "VERITAS", D. Serikbayev East Kazakhstan Technical University, Ust-Kamenogorsk, Kazakhstan

[2]Department of Automotive Engineering, Wrocław University of Science and Technology, Wrocław, Poland

*Corresponding author: Yerbolat Dias, e-mail: dyerbolat@edu.ektu.kz

Keywords:
WC-Fe alloys, WC-Ni alloys, mechanical activation, spark plasma sintering, cobalt-free hard alloys, nanocrystalline structure, microhardness, powder metallurgy.

ABSTRACT

The influence of mechanical activation and spark plasma sintering on the structural-phase state and mechanical properties of cobalt-free $WC_{95}Fe_5$ and $WC_{95}Ni_5$ hard alloys was investigated. Powder mixtures were prepared by high-energy milling in a planetary ball mill for 30 and 60 minutes. It was found that increasing the mechanical activation time leads to a decrease in crystallite size to 23.8-32.0 nm and an increase in microstrains to 0.198-0.222%. SPS sintering at temperatures of 1300-1350 °C is accompanied by partial relaxation of the defect structure and crystallite growth. The maximum relative density values were 90% for $WC_{95}Fe_5$ and 89% for $WC_{95}Ni_5$, and microhardness values were 1320 and 1080 HV, respectively. The WC-Fe system was shown to exhibit higher mechanical properties compared to WC-Ni. The obtained results indicate the promise of combining mechanical activation and SPS for producing cobalt-free hard alloys, but require further optimization of consolidation parameters.

INTRODUCTION

Tungsten carbide (WC) based hard alloys occupy a leading position in the modern tooling industry. Their high hardness, wear resistance, and ability to maintain performance at elevated temperatures make them indispensable for the production of cutting inserts, drill bits, and die tooling (Kurlov & Gusev, 2013; Lassner & Schubert, 1999; Mukhopadhyay & Basu, 2011). Cobalt is the classic binder component, providing excellent wetting of WC grains and thus enabling the formation of a dense composite with a good combination of mechanical properties (Armstrong, 2011). However, since the 2000s, the economic and environmental drawbacks of cobalt have become increasingly evident: its market price is highly volatile, resources are limited, and the inhalation of cobalt containing dust is associated with carcinogenic risks (Chang & Chen, 2014; He & Schoenung, 2002; Yang et al., 2020).

These circumstances drive researchers to search for alternative binder metals. Iron and nickel are considered the most justified candidates to replace Co. Both elements have melting points close to that of cobalt, are chemically compatible with WC, and can form a ductile γ phase that binds the carbide grains together (Voitovich et al., 1996; Zhong et al., 2015). Iron attracts attention due to its low cost and high carbon solubility, while nickel provides enhanced corrosion resistance and ductility. The literature reports that, under appropriately selected sintering conditions, WC-Fe and WC-Ni alloys can achieve mechanical properties comparable to those of

commercial WC-Co (Cai et al., 2017; García et al., 2019; Shichalin et al., 2022). At the same time, replacing cobalt with Fe or Ni demands more precise control of the technological parameters because of somewhat poorer wetting of carbide grains and a narrower temperature range for effective densification (Uazyrkhanova et al., 2025).

Powder mixture preparation plays a significant role in improving the quality of cobalt free composites. High energy mechanical activation in planetary ball mills has long proven to be a tool that sharply increases the homogeneity and reactivity of the charge (Suryanarayana, 2001). During repeated collisions, the WC, Fe and Ni particles are severely deformed, fragmented and locally welded together. The result is a uniform distribution of the binder, a reduction of crystallite size to the nanometer range, accumulation of defects, and consequently a marked lowering of the sintering temperatures (Gao et al., 2018; Lima et al., 2024; Zhang et al., 2024).

Nevertheless, the achievements obtained at the activation stage are easily nullified by conventional sintering methods. Long holding at high temperatures inevitably triggers recrystallization and uncontrolled grain growth, which cancels out the advantages of the nanostructured state (Munir, Anselmi-Tamburini, & Ohyanagi, 2006; Tokita, 2013). An effective way to solve this problem is spark plasma sintering (SPS). In SPS, heating is achieved by passing high density pulsed current through the graphite tooling and the powder, generating Joule heat directly inside the material. This arrangement allows heating rates as high as 1000 °C/min and shortens the holding time at the maximum temperature to a few minutes (Munir et al., 2006; Shichalin et al., 2020). As a result, grain coalescence can be almost completely suppressed, and the ultrafine structure formed during mechanical activation can be preserved (Genga et al., 2013; Lima et al., 2020).

The efficiency of combining SPS with prior mechanical activation has already been demonstrated for several carbide based compositions. For WC based systems, specimens with submicron grains have been obtained at temperatures 200-300 °C lower than those required in conventional sintering. It has been shown that an almost pore free state can be achieved while keeping the crystallite size at the nanometer level (Boukantar et al., 2020; da Silva et al., 2021; Rong et al., 2012). However, for composites with a low content of iron and nickel binder, systematic data on the combined effect of mechanical activation time and SPS temperature on the final properties are lacking. This is especially true for a direct comparative analysis of the two alternative systems, WC-Fe and WC-Ni, under identical processing conditions - which constitutes the scientific novelty of the present work.

The aim of this study is to establish the regularities of structure formation and the physical-mechanical properties of WC-5 at.% Fe and WC-5 at.% Ni alloys as a function of mechanical activation time and spark plasma sintering temperature.

MATERIALS AND METHODS

Elemental powders of WC (purity > 99.9%, particle size < 30 μm), Fe (purity > 99.9%, particle size < 30 μm), and Ni (purity > 99.9%, particle size < 50 μm) were used as starting materials. The powders were supplied by Hebei Suoyi New Material Technology Co., Ltd. (Handan City, Hebei Province, China).

The morphology of the initial WC, Fe, and Ni powders is shown in Figure 1. Tungsten carbide powder exhibits angular particle shapes with distinct facets and sharp edges, which is typical for brittle ceramic materials. The particles have a relatively wide size distribution and show a slight tendency to agglomerate due to their high specific surface area. Iron powder features more rounded and smoothed particle shapes. Both individual particles and small agglomerates are observed. The particle surface is relatively flat, which is attributed to the ductility of the material and the specifics of its production. Nickel powder is characterized by predominantly rounded or slightly elongated particles with a smooth surface. The particles are distributed rather uniformly, with no pronounced agglomeration.

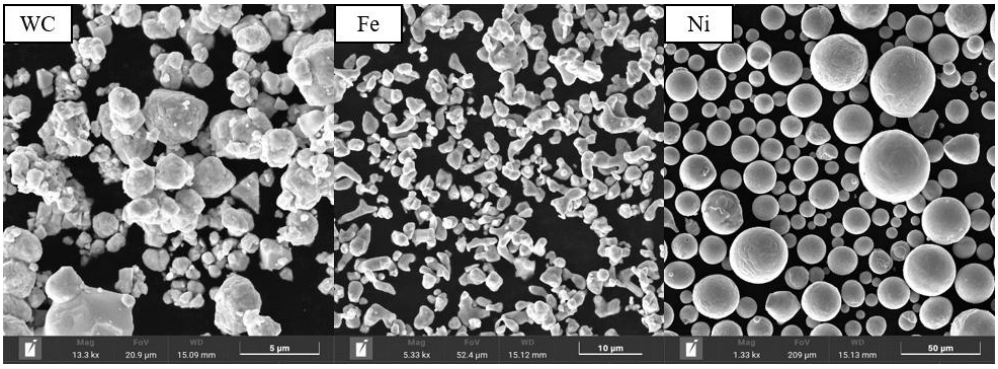

Figure 1. Initial powders

Note – compiled by the author

The initial powders with nominal compositions of $WC_{95}Fe_5$ and $WC_{95}Ni_5$ (at.%) were subjected to high-energy milling in a planetary ball mill Fritsch Pulverisette 7 premium line (Fritsch GmbH, Idar-Oberstein, Germany). Steel balls of 5 mm diameter were used as grinding media, and the volume of the milling vials was 45 mL. The ball-to-powder mass ratio was 10:1. The milling duration was 30 and 60 minutes at a rotation speed of 650 rpm, with 5-minute pauses every 10 minutes of operation to prevent local overheating inside the milling vials. To reduce agglomeration during milling, a small amount of stearic acid (2.5% of the powder mass) was added. The process was carried out in an inert argon atmosphere. The loading and unloading of powder mixtures into and from the planetary mill were performed in a vacuum glove box to prevent oxidation. Powder blending was also carried out for 10 minutes at a rotation speed of 200 rpm without the addition of stearic acid.

The powder mixtures obtained after mechanical activation were sintered by spark plasma sintering using a U-Fast Compact 40 Pro (Genicore, Poland). Sintering was carried out at temperatures of 1300 and 1350 °C under uniaxial pressure of 30 MPa. The heating rate was 100 °C/min, and the holding time at the maximum temperature was 7 min. The process was conducted in a graphite mold with a diameter of 20 mm. The mass of the powder mixture before sintering was 25 g. Sintering was performed in a vacuum atmosphere with a residual pressure of about 5×10^{-2} mbar.

Annealing of the samples was carried out in an atmosphere furnace (model SA2-4-17TP, Hefei Kejing Materials Technology Co., Ltd., China) at 500 °C with a holding time of 60 min to relieve residual stresses. The heating rate was 20 °C/min. The heat treatment was performed under vacuum. After the holding time, the samples were cooled together with the furnace and removed after complete cooling to room temperature. After heat treatment, the samples were ground to prepare the surface for subsequent studies.

Powder morphology was analyzed using a TESCAN MIRA LMS scanning electron microscope (TESCAN, Brno, Czech Republic).

The particle size of the milled powders was determined using a Fritsch Analysette 22 NEXT particle size analyzer (Fritsch GmbH, Idar-Oberstein, Germany).

The crystal structure of the milled powders was investigated using an X'Pert PRO X-ray diffractometer (Malvern Panalytical Empyrean, Almelo, The Netherlands) with a copper anode (CuKα1, λ = 1.5406 Å). The measurement range was 20-90°, the X-ray tube voltage was 40 kV, and the current was 30 mA. The scanning step was 0.02°, with a counting time of 1 s per step. A fixed divergence slit of 1/2°, a distance of 91 mm from the divergence slit to the tube focus, a fixed incident mask of 15 mm, and an anti-scatter slit of 2° were used. All measurements were carried out at a temperature of 25 °C. Diffractogram processing was performed using HighScore software (version 4.9a, 2021). Phase analysis was carried out using the PDF 5 database (2025).

The average crystallite size and microstrain were determined using the classical Williamson-Hall method, which takes into account the contribution of finite crystallite size and microstrains to the broadening of X-ray peaks. The full width at half maximum (FWHM, β) of the diffraction peaks was corrected for instrumental broadening. The Williamson-Hall equation is as follows:

$$\beta(2\theta) = k\lambda/D\cos\theta + 4\varepsilon\tan\theta \quad (1)$$

The relative density of the sintered samples was determined by the Archimedes method using hydrostatic weighing.

The microhardness of the samples was determined by the Vickers method using a DuraScan 20 (EMCO-TEST Prüfmaschinen GmbH, Austria). The tests were carried out at a load of 1 kg and a holding time of 10 s.

RESULTS AND DISCUSSION

The microstructure of $WC_{95}Fe_5$ and $WC_{95}Ni_5$ powder mixtures at various stages of mechanical activation is shown in Figures 2 and 3.

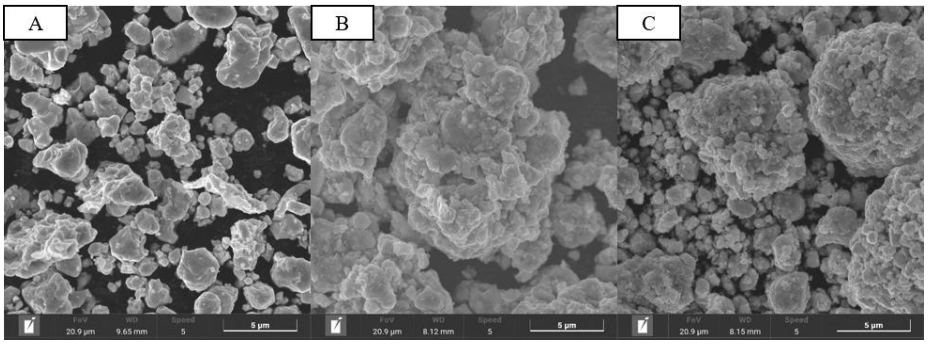

Figure 2. $WC_{95}Fe_5$ powder mixture: a) after mixing, b) after 30 min of mechanical activation, c) after 60 min of mechanical activation (magnification ×10000)

Note – compiled by the author

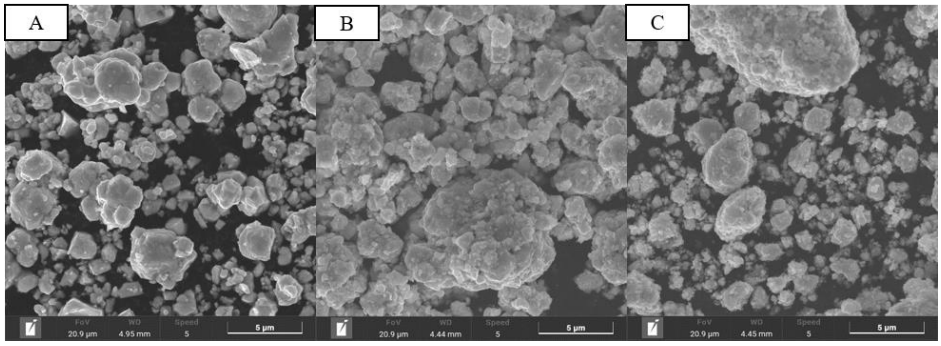

Figure 3. $WC_{95}Ni_5$ powder mixture: a) after mixing, b) after 30 min of mechanical activation, c) after 60 min of mechanical activation (magnification ×10000)

Note – compiled by the author

For both systems after the mixing stage (Figures 2a, 3a), the retention of the initial powder morphology is characteristic: angular tungsten carbide grains are uniformly distributed throughout the volume, and particles of the metallic binder (Fe or Ni) are located between them. Agglomeration is weak, and the structure is relatively homogeneous and dispersed.

After 30 minutes of mechanical activation (Figures 2b, 3b), a significant change in morphology is observed in both systems. Large, irregularly shaped agglomerates are formed due to the intensive occurrence of cold welding processes. Moreover, for the WC95Ni5 system, this effect is more pronounced, which is associated with the higher ductility of nickel compared to iron, promoting more effective particle bonding and the formation of dense conglomerates. As a result, the structure becomes inhomogeneous and characterized by a wide particle size distribution.

Upon increasing the mechanical activation duration to 60 minutes (Figures 2c, 3c), the destruction of previously formed agglomerates is observed in both systems. The particles acquire a more compact shape, the proportion of large conglomerates decreases, and the structure becomes more homogeneous. For the $WC_{95}Ni_5$ system, this process proceeds more efficiently, which is manifested in the formation of a finer structure compared to $WC_{95}Fe_5$. This indicates the transition of the mechanical activation process to the stage of dynamic equilibrium between cold welding and particle fracture.

Table 1. Average particle size of $WC_{95}Fe_5$ and $WC_{95}Ni_5$ depending on the mechanical activation time

Powder mixture	Average particle size, μm		
	as-mixed	30 min	60 min
$WC_{95}Fe_5$	2,737±0,0324	19,045±0,4830	5,817±0,4492
$WC_{95}Ni_5$	2,467±0,0301	20,699±0,1563	3,803±0,2860
Note – compiled by the author			

The observed morphological changes are consistent with the evolution of the mean particle size (Table 1). For the $WC_{95}Fe_5$ system, the mean particle size after mixing is about 2.7 μm; after 30 minutes of mechanical activation it increases to ~19.0 μm due to agglomeration; and upon increasing the time to 60 minutes it decreases to ~5.8 μm because of agglomerate disintegration. A similar trend is observed for the $WC_{95}Ni_5$ system: after mixing the mean particle size is about 2.5 μm, then it increases to ~20.7 μm after 30 minutes of mechanical activation and decreases to ~3.8 μm after 60 minutes of processing. The lower mean particle size for the $WC_{95}Ni_5$ system indicates more efficient comminution, which is consistent with the SEM analysis results.

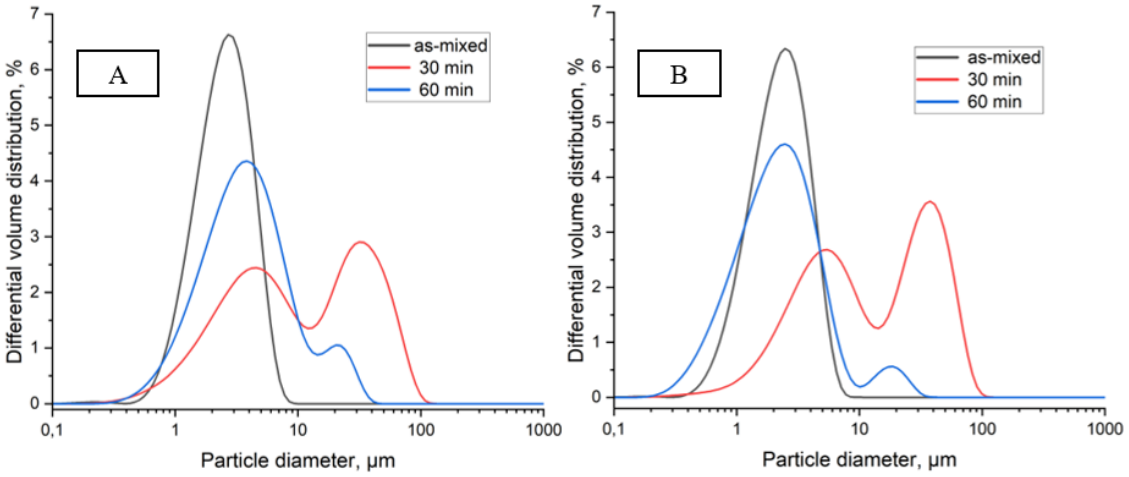

Figure 4. Particle size distribution of the (a) $WC_{95}Fe_5$ and (b) $WC_{95}Ni_5$ powder mixtures after different mechanical activation times

Note – compiled by the author

The particle size distribution analysis (Fig. 4) confirms the revealed trends. For both systems after mixing, the distributions are narrow and concentrated in the fine size range, indicating high powder homogeneity. After 30 minutes of mechanical activation, the distributions broaden substantially and shift toward larger sizes, acquiring a polymodal character, which is associated with the formation of agglomerates. Upon increasing the time to 60 minutes, the distributions narrow again and shift toward smaller sizes, indicating the disintegration of agglomerates and an improvement in structural homogeneity. Moreover, for the $WC_{95}Ni_5$ system, a narrower distribution is observed compared to $WC_{95}Fe_5$, pointing to a higher degree of powder dispersion and homogenization.

Thus, it has been established that increasing the mechanical activation duration to 60 minutes leads to the formation of a more homogeneous and fine-grained structure in both systems, while the use of nickel as a binder phase provides more efficient comminution and a narrower particle size distribution.

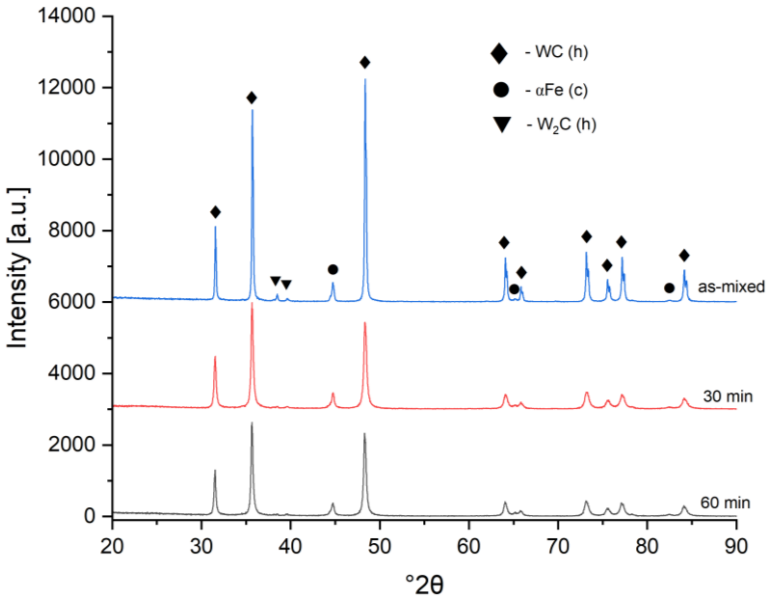

Figure 5. X-ray diffraction patterns of $WC_{95}Fe_5$ powder mixtures after different mechanical activation times

Note – compiled by the author

On the X-ray diffraction patterns of the $WC_{95}Fe_5$ powder mixture (Fig. 5) after the mixing stage, intense and narrow diffraction peaks corresponding WC, W_2C and Fe are observed, indicating a high degree of crystallinity of the initial powders. The average crystallite size is 86.8 nm, and the microstrain value is 0.052%, which points to a low level of structural defectiveness.

After 30 minutes of mechanical activation, a noticeable broadening of the diffraction peaks and a decrease in their intensity are observed. This is associated with a reduction in crystallite size to 37.8 nm and an increase in microstrains to 0.163% (Fig. 7) due to intensive plastic deformation and defect accumulation. A decrease in the intensity of the iron peaks is also noted, which may be related to its more uniform distribution within the WC matrix.

Upon increasing the mechanical activation time to 60 minutes, the peak broadening becomes more pronounced, and their intensity continues to decrease. The average crystallite size decreases to 32.0 nm, while microstrains increase to 0.198% (Fig. 7). This indicates further structural refinement and accumulation of crystal lattice defects.

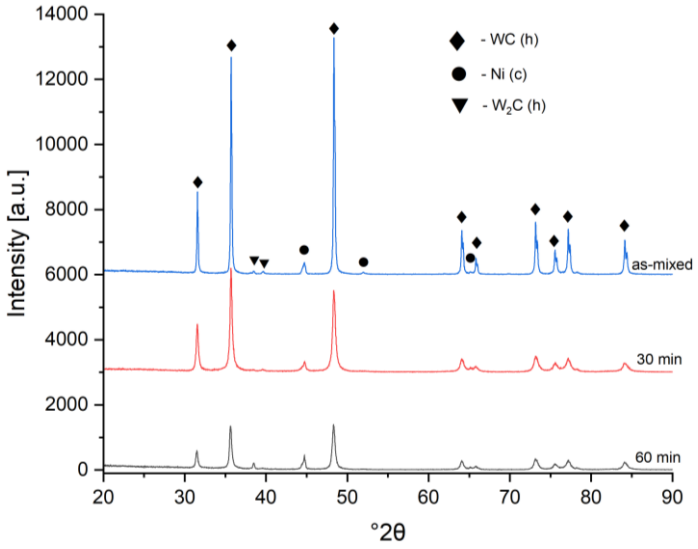

Figure 6. X-ray diffraction patterns of $WC_{95}Ni_5$ powder mixtures after different mechanical activation times

Note – compiled by the author

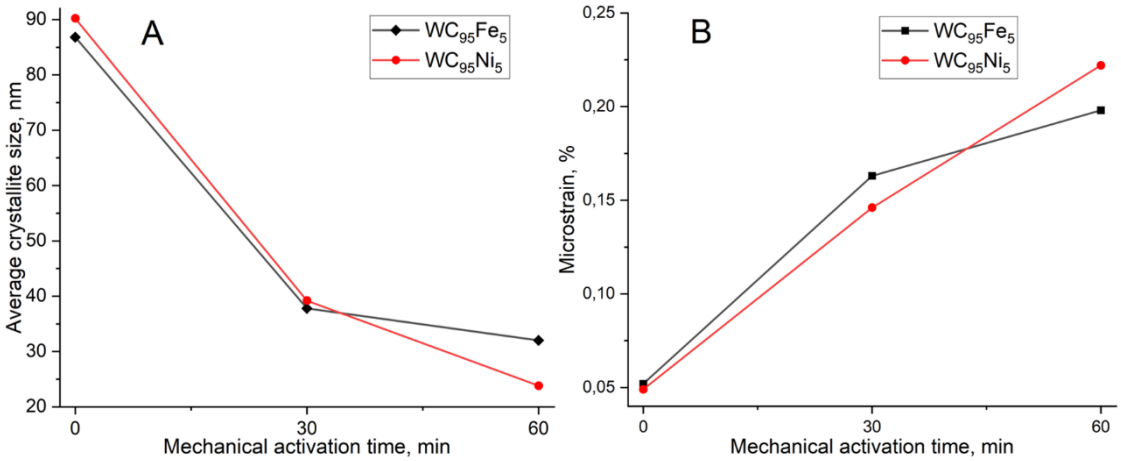

Figure 7. Average crystallite size and microstrain of $WC_{95}Fe_5$ and $WC_{95}Ni_5$ powder mixtures after different mechanical activation times: (a) average crystallite size, (b) microstrain

Note – compiled by the author

For the $WC_{95}Ni_5$ system (Fig. 6) after mixing, narrow and intense peaks of WC, W_2C and Ni, characteristic of crystalline starting powders, are also observed. The average crystallite size is 90.2 nm, and the microstrains are 0.049% (Fig. 7), corresponding to a low level of internal stresses.

After 30 minutes of mechanical activation, peak broadening and a decrease in their intensity occur, which is more pronounced compared to the $WC_{95}Fe_5$ system. The crystallite size decreases to 39.2 nm, and microstrains increase to 0.146% (Fig. 7). The more intensive structural change is due to the high ductility of nickel, which promotes defect accumulation.

After 60 minutes of mechanical activation, significant broadening of the diffraction peaks and a further decrease in their intensity are observed. The average crystallite size decreases to 23.8 nm, and microstrains increase to 0.222% (Fig. 7). This indicates more intensive structural refinement and a higher level of defectiveness compared to the $WC_{95}Fe_5$ system.

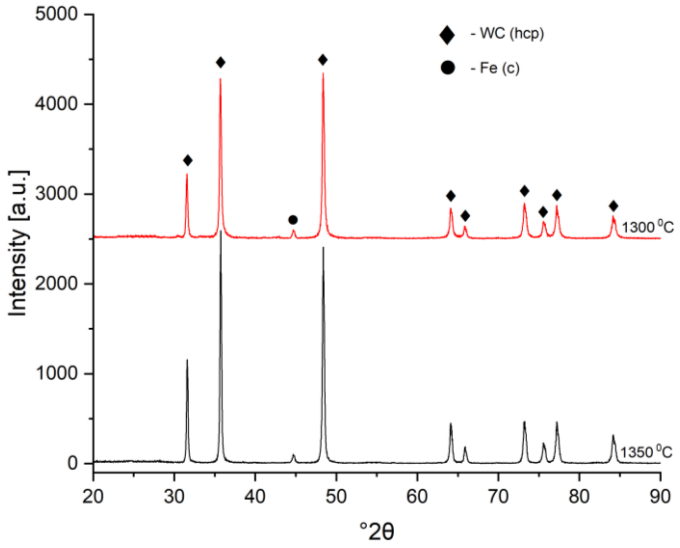

Figure 8. X-ray diffraction patterns of $WC_{95}Fe_5$ after sintering
Note – compiled by the author

In the X-ray diffraction patterns of sintered samples of the $WC_{95}Fe_5$ system (Fig. 8), characteristic peaks of hexagonal WC and the face-centered cubic Fe phase are observed. Compared to the state after mechanical activation, these peaks exhibit a noticeable narrowing and an increase in intensity. These changes indicate a partial recovery of the crystalline structure during spark plasma sintering and a reduction in the degree of structural defectiveness. As the sintering temperature increases from 1300 to 1350 °C, further narrowing of the diffraction peaks occurs, reflecting an increase in the average crystallite size from 56.8 to 67.8 nm, according to the data in Fig. 10a. Simultaneously, a decrease in the microstrain level from 0.092% to 0.079% (Fig. 10b) is observed, which is attributed to the relaxation of crystal lattice defects accumulated during mechanical activation and the reduction of internal stresses. Thus, for the $WC_{95}Fe_5$ system, an increase in sintering temperature is accompanied by pronounced recrystallization and grain growth processes, along with a decrease in structural defectiveness.

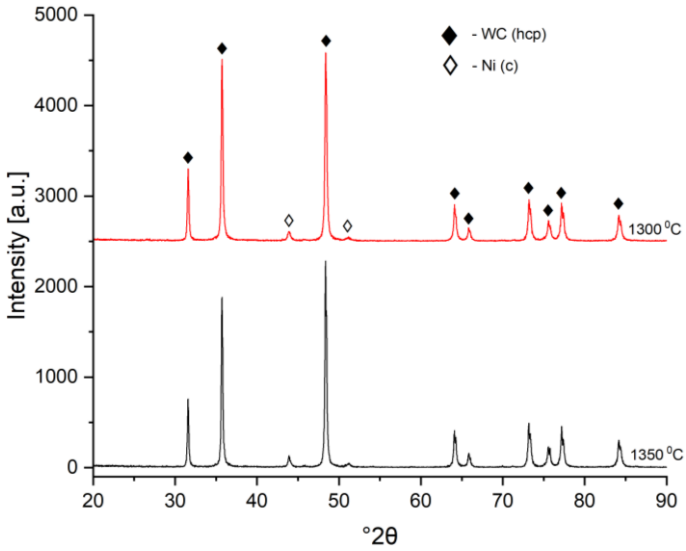

Figure 9. X-ray diffraction patterns of $WC_{95}Ni_5$ after sintering
Note – compiled by the author

For the $WC_{95}Ni_5$ system (Fig. 9), similar trends in the evolution of X-ray diffraction characteristics after sintering are observed, although their magnitude is somewhat different. The diffraction peaks of hexagonal WC and the face-centered cubic Ni phase also become narrower and more intense compared to the powder state, indicating the restoration of crystalline order. As the sintering temperature increases from 1300 to 1350 °C, the average crystallite size increases from 58.2 to 63.2 nm (Fig. 10a); however, the increase is less significant than that for the $WC_{95}Fe_5$ system. Concurrently, the microstrain level decreases from 0.089% to 0.083% (Fig. 10b), indicating partial relaxation of defects, although this process proceeds less intensively. The retention of a lower crystallite growth rate in the WC95Ni5 system may be associated with the more ductile nature of the nickel binder phase, which hinders intensive grain coalescence and promotes the retention of a more dispersed structure.

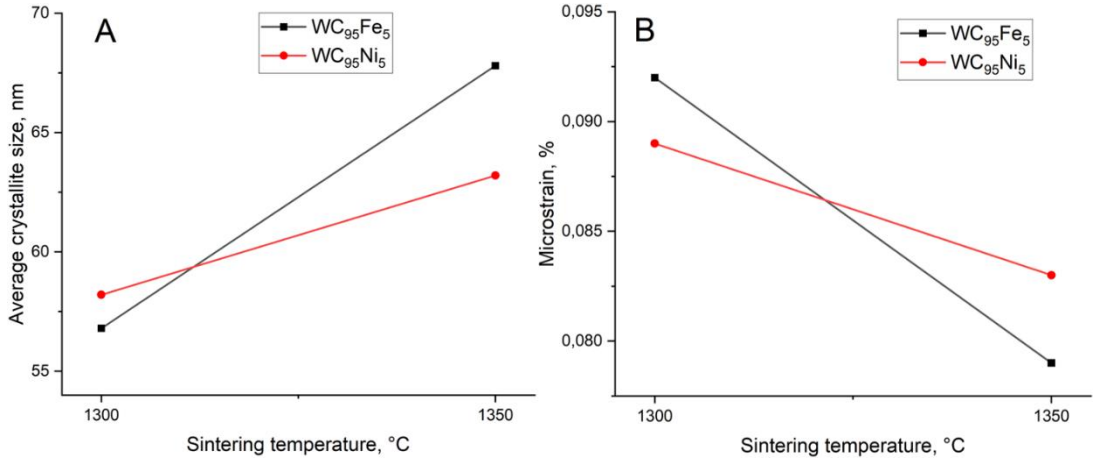

Figure 10. Average crystallite size and microstrain of sintered $WC_{95}Fe_5$ and $WC_{95}Ni_5$ samples: (a) average crystallite size, (b) microstrain

Note – compiled by the author

Table 2. Microhardness (Vickers) and relative density values of sintered $WC_{95}Fe_5$ and $WC_{95}Ni_5$ samples.

Sintering temperature	Microhardness, HV		Relative density, %	
	$WC_{95}Fe_5$	$WC_{95}Ni_5$	$WC_{95}Fe_5$	$WC_{95}Ni_5$
1300 °C	1180	950	86	85
1350 °C	1320	1080	90	89
Note – compiled by the author				

Analysis of the data presented in Table 2 reveals a correlation between the relative density and microhardness of the sintered samples. For the $WC_{95}Fe_5$ system, at a sintering temperature of 1300 °C, the relative density is 86%, while the microhardness reaches 1180 HV. Upon increasing the temperature to 1350 °C, the density increases to 90%, which is accompanied by a rise in microhardness to 1320 HV. A similar dependence is observed for the $WC_{95}Ni_5$ system: at 1300 °C, the relative density is 85% and the microhardness is 950 HV, whereas at 1350 °C, the density increases to 89% and microhardness rises to 1080 HV. These results indicate that an increase in sintering temperature leads to more effective material densification, a reduction in porosity, and consequently, an increase in microhardness. In all cases, the $WC_{95}Fe_5$ system

exhibits higher values of both density and microhardness compared to the $WC_{95}Ni_5$ system, which is attributed to the more rigid nature of the iron binder phase relative to the nickel binder.

It should be noted that the mechanical activation and spark plasma sintering parameters employed in this work are not optimal with respect to achieving maximum density. In particular, the relatively short holding time during SPS (7 min) was deliberately chosen to limit grain growth and preserve the fine-grained structure formed during the mechanical activation stage.

It is known that increasing the temperature and holding time during SPS leads to more complete material consolidation by activating diffusion processes and reducing porosity. However, such conditions are generally accompanied by coarsening of the grain structure, which may negate the advantages obtained from mechanical activation. In this regard, the implemented sintering regime can be considered a compromise between the degree of densification and the retention of a fine-grained state. The obtained values of relative density and microhardness in this case are due to the limited sintering duration and, consequently, the incomplete realization of diffusion-controlled densification processes. Further improvements in density and mechanical properties are possible by increasing the holding time, sintering temperature, or the binder phase content; however, this would likely lead to grain growth. Therefore, optimization of the SPS parameters in the studied systems requires a balance between retaining the fine-grained structure and achieving a high degree of densification.

CONCLUSIONS

It has been established that increasing the mechanical activation time to 60 minutes leads to the formation of a nanostructured state in WC-Fe and WC-Ni powder mixtures. For the system with a nickel binder, the crystallite size decreases to 23.8 nm, and microstrains reach 0.222%, whereas for WC-Fe, these values are 32.0 nm and 0.198%, respectively, with the higher ductility of nickel promoting intensive accumulation of crystal lattice defects. Spark plasma sintering at temperatures of 1300-1350 °C with a short holding time of 7 minutes allows for partial relaxation of the defective structure and preserves the fine-grained state of the materials. Increasing the sintering temperature enhances the relative density: from 86% to 90% for WC-Fe, and from 85% to 89% for WC-Ni. This is accompanied by an increase in microhardness: from 1180 to 1320 HV for WC-Fe, and from 950 to 1080 HV for WC-Ni. The WC-Fe system exhibits higher density and hardness across all regimes due to the specific behavior of the iron binder phase. The obtained density and hardness values are consistent with the selected sintering regimes, which are designed to suppress grain growth and preserve the nanostructure, and do not represent the maximum achievable values.

The scientific novelty of this research lies in demonstrating that the combination of mechanical activation for 60 minutes followed by spark plasma sintering at 1350 °C with a short holding time provides a viable compromise between densification and nanostructure retention in cobalt-free cemented carbides. The theoretical conclusion is that the more rigid iron binder phase promotes higher densification and hardness, while the more ductile nickel binder phase better suppresses grain growth, offering a guideline for binder selection based on the desired microstructure.

The practical significance is that the proposed processing route represents a promising approach for producing cobalt-free WC-Fe and WC-Ni cemented carbides with controlled nanostructure. A limitation identified is that the short holding time prevents full diffusion-controlled densification, and achieving properties comparable to cobalt-based analogues would require further optimization of consolidation parameters.

Prospects for further research include optimizing sintering temperature, holding time, or uniaxial pressure to achieve higher density and hardness while maintaining nanostructure, as well as examining wear resistance, fracture toughness, and hybrid Fe-Ni binder compositions.

CONFLICT OF INTEREST: The authors declare no conflict of interest.

FUNDING: This research is funded by the Committee of Science of the Ministry of Science and Higher Education of the Republic of Kazakhstan under the topic BR24992925 "Development of technology and materials for the innovative development of the manufacturing industry of the Republic of Kazakhstan".

INSTITUTIONAL REVIEW BOARD STATEMENT: Not applicable. This study did not involve humans or animals.

INFORMED CONSENT STATEMENT: Not applicable. This study did not involve human participants.

DATA AVAILABILITY STATEMENT: The data supporting the findings of this study are available from the corresponding author upon reasonable request.

ACKNOWLEDGEMENTS: The authors thank the anonymous reviewers for their constructive comments.

STATEMENT ON THE USE OF ARTIFICIAL INTELLIGENCE TECHNOLOGIES: The authors used artificial intelligence tools – ChatGPT (OpenAI, GPT-4o) and DeepSeek (DeepSeek-R1) - to assist with language editing, text structuring, and improving the clarity of the manuscript. All scientific content, data analysis, and conclusions were developed and verified by the authors, who take full responsibility for the integrity of the work.

REFERENCES

Kurlov, A. S., & Gusev, A. I. (2013). Tungsten Carbides and W-Co Hardmetals. Springer. https://doi.org/10.1007/978-3-319-00524-9

Lassner, E., & Schubert, W. D. (1999). Tungsten: Properties, Chemistry, Technology of the Element, Alloys, and Chemical Compounds. Springer. https://doi.org/10.1007/978-1-4615-4907-9

Mukhopadhyay, A., & Basu, B. (2011). Recent developments on WC-based bulk composites. Journal of Materials Science, 46(3), 571-589. https://doi.org/10.1007/s10853-010-5046-7

Armstrong, R. W. (2011). The Hardness and Strength Properties of WC-Co Composites. Materials, 4(7), 1287-1308. https://doi.org/10.3390/ma4071287

He, J., & Schoenung, J. M. (2002). A review on nanostructured WC-Co coatings. Surface and Coatings Technology, 157(1), 72-79. https://doi.org/10.1016/S0257-8972(02)00141-X

Yang, Y., Zhang, C., Wang, D., Nie, L., Wellmann, D., & Tian, Y. (2020). Additive manufacturing of WC-Co hardmetals: a review. The International Journal of Advanced Manufacturing Technology, 108(5-6), 1653-1673. https://doi.org/10.1007/s00170-020-05389-5

Chang, S.-H., & Chen, S.-L. (2014). Characterization and properties of sintered WC-Co and WC-Ni-Fe hard metal alloys. Journal of Alloys and Compounds, 585, 407-413. https://doi.org/10.1016/j.jallcom.2013.09.188

Voitovich, V. B., Sverdel, V. V., Voitovich, R. F., & Golovko, É. I. (1996). Oxidation of WC-Co, WC-Ni and WC-Co-Ni hard metals in the temperature range 500-800 °C. International Journal of Refractory Metals and Hard Materials, 14(4), 289-295. https://doi.org/10.1016/0263-4368(96)00009-1

Zhong, L., Xu, Y., Hojamberdiev, M., & Liu, J. (2015). Microstructural and Mechanical Properties of In Situ WC-Fe/Fe Composites. Journal of Materials Engineering and Performance, 24(11), 4561-4568. https://doi.org/10.1007/s11665-015-1742-4

Shichalin, O. O., Buravlev, I. Yu., Papynov, E. K., et al. (2022). Comparative study of WC-based hard alloys fabrication via spark plasma sintering using Co, Fe, Ni, Cr, and Ti binders. International Journal of Refractory Metals and Hard Materials, 102, 105725. https://doi.org/10.1016/j.ijrmhm.2021.105725

García, J., Collado Ciprés, V., Blomqvist, A., & Kaplan, B. (2019). Cemented carbide microstructures: a review. International Journal of Refractory Metals and Hard Materials, 80, 40-68. https://doi.org/10.1016/j.ijrmhm.2018.12.004

Cai, X., Xu, Y., Zhong, L., & Liu, M. (2017). Fracture toughness of WC-Fe cermet in W-WC-Fe composite by nanoindentation. Journal of Alloys and Compounds, 728, 788-796. https://doi.org/10.1016/j.jallcom.2017.09.070

Uazyrkhanova, G., Kozhakhmetov, Y., Aidarova, M., Rutkowska-Gorczyca, M., & Tabiyeva, Y. (2025). Combined Approach to the Synthesis of WC-(Fe, Ni) Hard Alloys: Mechanical Activation and Spark Plasma Sintering. Crystals, 15(8), 724. https://doi.org/10.3390/cryst15080724

Suryanarayana, C. (2001). Mechanical alloying and milling. Progress in Materials Science, 46(1-2), 1-184. https://doi.org/10.1016/S0079-6425(99)00010-5

Zhang, Z., et al. (2024). Effect of W-to-C atomic ratio on microstructure and properties of in-situ synthesized WC/Fe composites by spark plasma sintering. International Journal of Refractory Metals and Hard Materials, 121, 106643. https://doi.org/10.1016/j.ijrmhm.2024.106643

Gao, Y., Luo, B.-H., He, K.-J., Zhang, W.-W., & Bai, Z.-H. (2018). Effect of Fe/Ni ratio on the microstructure and properties of WC-Fe-Ni-Co cemented carbides. Ceramics International, 44(3), 3291-3296. https://doi.org/10.1016/j.ceramint.2017.10.148

Lima, M. J. S., Silva, F. E. S., Raimundo, R. A., et al. (2024). Enhanced properties of hard metal WC-Ni processed from nanostructured powders. Ceramics International, 50(22, Part B), 47445-47455. https://doi.org/10.1016/j.ceramint.2024.09.096

Zhang, Z., et al. (2017). The effect of volume fraction of WC particles on wear behavior of in-situ WC/Fe composites by spark plasma sintering. International Journal of Refractory Metals and Hard Materials, 69, 196-208. https://doi.org/10.1016/j.ijrmhm.2017.08.009

Guillon, O., et al. (2014). Field-Assisted Sintering Technology/Spark Plasma Sintering: Mechanisms, Materials, and Technology Developments. Advanced Engineering Materials, 16(7), 830-849. https://doi.org/10.1002/adem.201300409

Munir, Z. A., Anselmi-Tamburini, U., & Ohyanagi, M. (2006). The effect of electric field and pressure on the synthesis and consolidation of materials: A review of the spark plasma sintering method. Journal of Materials Science, 41(3), 763-777. https://doi.org/10.1007/s10853-006-6555-2

Tokita, M. (2013). Spark Plasma Sintering (SPS) Method, Systems, and Applications. In Handbook of Advanced Ceramics (2nd ed., pp. 1149-1177). Academic Press. https://doi.org/10.1016/B978-0-12-385469-8.00060-5

Munir, Z. A., Ohyanagi, M., Tokita, M., Khor, M., Hirai, T., & Anselmi-Tamburini, U. (Eds.). (2006). Pulse Electric Current Synthesis and Processing of Materials (Ceramic Transactions, Vol. 194). American Ceramic Society; Wiley-Interscience.

Shichalin, O. O., et al. (2020). SPS hard metal alloy WC-8Ni-8Fe fabrication based on mechanochemical synthetic tungsten carbide powder. Journal of Alloys and Compounds, 816, 152547. https://doi.org/10.1016/j.jallcom.2019.152547

Lima, M. J. S., Silva, F. E. S., Lima, H. D., Souto, M. V. M., Oliveira, A. G. F., Raimundo, R. A., Souza, C. P., & Gomes, U. U. (2020). Spark plasma sintering of nanostructured powder composites (WC-Ni) prepared by carboreduction reaction. Materials Chemistry and Physics, 254, 123439. https://doi.org/10.1016/j.matchemphys.2020.123439

Genga, R. M., Cornish, L. A., & Akdogan, G. (2013). Effect of Mo_2C additions on the properties of SPS manufactured WC-TiC-Ni cemented carbides. International Journal of Refractory Metals and Hard Materials, 41, 12-21. https://doi.org/10.1016/j.ijrmhm.2013.01.008

Rong, H., Peng, Z., Ren, X., Peng, Y., & Wang, C. (2012). Ultrafine WC-Ni cemented carbides fabricated by spark plasma sintering. Materials Science and Engineering: A, 532, 543-547. https://doi.org/10.1016/j.msea.2011.10.119

da Silva, E. N., dos Santos, A. A. A., do Nascimento, R. M., Alves, S. M., da Silva Guimarães, R., & Filgueira, M. (2021). Investigation of characteristics and properties of spark plasma sintered ultrafine WC-6.4Fe3.6Ni alloy as potential alternative WC-Co hard metals. International Journal of Refractory Metals and Hard Materials, 101, 105669. https://doi.org/10.1016/j.ijrmhm.2021.105669

Boukantar, A.-R., Djerdjare, B., Guiberteau, F., & Ortiz, A. L. (2020). Spark plasma sinterability and dry sliding-wear resistance of WC densified with Co, Co+Ni, and Co+Ni+Cr. International Journal of Refractory Metals and Hard Materials, 92, 105280. https://doi.org/10.1016/j.ijrmhm.2020.105280

Information about authors

Yerkezhan Tabiyeva – Center of Excellence "VERITAS", D. Serikbayev East Kazakhstan Technical University, Ust-Kamenogorsk, Kazakhstan. PhD in Technical Physics.
Powder metallurgy, alloys, mechanical alloying
E-mail: etabieva@edu.ektu.kz
ORCID: https://orcid.org/0000-0002-9726-7187

Dias Yerbolat – Center of Excellence "VERITAS", D. Serikbayev East Kazakhstan Technical University, Ust-Kamenogorsk, Kazakhstan
Education: PhD student at the S. Amanzholov East Kazakhstan University (EKU) Ust-Kamenogorsk, Kazakhstan 2023 - Present. M.Sc. in Technical Sciences: D. Serikbayev East Kazakhstan Technical University (EKTU) 2021 - 2023. B.Sc.in automation and management: Al-Farabi Kazakh National University Almaty, Kazakhstan 2018 - 2021.
Powder metallurgy, alloys, ceramics, composite materials, XRD, spark plasma sintering, mechanical alloying
E-mail: dyerbolat@edu.ektu.kz
ORCID: https://orcid.org/0000-0002-2072-4212

Azamat Urkunbay – Center of Excellence "VERITAS", D. Serikbayev East Kazakhstan Technical University, Ust-Kamenogorsk, Kazakhstan. M.Sc. in Physics in Technical Physics Sarsen Amanzholov East Kazakhstan University, Ust-Kamenogorsk, Kazakhstan 2025 - Present. Bachelor's degree: Graduated with a bachelor's degree from the Kazakh University of Ways and Communications, majoring in Automation and Control
Powder metallurgy, alloys, spark plasma sintering, mechanical alloying
E-mail: aurkunbay@edu.ektu.kz
ORCID: https://orcid.org/0000-0002-7868-2393

Madina Aidarova – Center of Excellence "VERITAS", D. Serikbayev East Kazakhstan Technical University, Ust-Kamenogorsk, Kazakhstan. PhD student at the East Kazakhstan Technical University named after D. Serikbaev, Ust-Kamenogorsk, Kazakhstan. 2012-2016 - Bachelor's degree in 5B072300 Technical Physics, Shakarim State University of Semey. 2016-2018 - Master's degree in 6M072300 Technical Physics, Shakarim State University of Semey. Powder metallurgy, alloys, mechanical alloying
E-mail: maidarova@edu.ektu.kz
ORCID: https://orcid.org/0009-0000-9200-8058

Sayat Zakerov – Center of Excellence "VERITAS", D. Serikbayev East Kazakhstan Technical University, Ust-Kamenogorsk, Kazakhstan. M.Sc. in Technical Physics at the D. Serikbayev East Kazakhstan Technical University (EKTU), Ust-Kamenogorsk, Kazakhstan 2024 - Present. B.Sc. in Physics D. Serikbayev East Kazakhstan Technical University (EKTU), Ust-Kamenogorsk, Kazakhstan 2020 – 2024. Powder metallurgy, alloys, spark plasma sintering, mechanical alloying
E-mail: szakerov@edu.ektu.kz
ORCID: https://orcid.org/0009-0000-9470-9018

Małgorzata Rutkowska-Gorczyca – Department of Automotive Engineering, Wrocław University of Science and Technology, Wrocław, Poland
PhD in Mechanics, Associate Professor.
Microstructure, material characterization, advanced materials, alloys
E-mail: malgorzata.rutkowska-gorczyca@pwr.edu.pl
ORCID: https://orcid.org/0000-0003-2712-5914